

This is a preprint of an article published in *Plant Physiology*. The final authenticated version is available online at: <https://doi.org/10.1093/plphys/kiab533>

## An *in situ* sequencing approach maps *PLASTOCHRON1* at the boundary between indeterminate and determinate cells

Reinout Laureyns<sup>1,2</sup>, Jessica Joossens<sup>1,2</sup>, Denia Herwegh<sup>1,2</sup>, Julie Pevernagie<sup>1,2</sup>, Benjamin Pavie<sup>3,4,5</sup>, Kirin Demuyne<sup>1,2</sup>, Kevin Debray<sup>1,2</sup>, Griet Coussens<sup>1,2</sup>, Laurens Pauwels<sup>1,2</sup>, Tom Van Hautegeem<sup>1,2</sup>, Michiel Bontinck<sup>6</sup>, Josh Strable<sup>7</sup> and Hilde Nelissen<sup>1,2,&</sup>

<sup>1</sup> Ghent University, Department of Plant Biotechnology and Bioinformatics, 9052 Ghent, Belgium

<sup>2</sup> VIB Center for Plant Systems Biology, 9052 Ghent, Belgium

<sup>3</sup> VIB Center for Brain & Disease Research, Leuven, Belgium;

<sup>4</sup> KU Leuven, Department of Neurosciences, Leuven Brain Institute, Leuven 3000, Belgium;

<sup>5</sup> VIB Bio Imaging Core, Gent 9052, Belgium; VIB Bio Imaging Core, Leuven 3000, Belgium.

<sup>6</sup> VIB Tech Watch team, 9052 Ghent, Belgium

<sup>7</sup> Department of Molecular and Structural Biochemistry, North Carolina State University, Raleigh, NC, USA 27695

& corresponding author [Hilde.Nelissen@psb.vib-ugent.be](mailto:Hilde.Nelissen@psb.vib-ugent.be)

### Abstract

The plant shoot apex houses the shoot apical meristem, a highly organized and active stem-cell tissue where molecular signaling in discrete cells determines when and where leaves are initiated. We optimized a spatial transcriptomics approach, *in situ* sequencing to colocalize the transcripts of 90 genes simultaneously on the same section of tissue from the maize shoot apex. The RNA *in situ* sequencing technology reported expression profiles that were highly comparable with those obtained by *in situ* hybridizations and allowed the discrimination between tissue domains. Furthermore, the application of spatial transcriptomics to the shoot apex, which is inherently comprised of phytomers that are in gradual developmental stages, provided a spatiotemporal sequence of transcriptional events. We illustrate the power of the technology through *PLASTOCHRON1* (*PLA1*) that is specifically expressed at the boundary between indeterminate and determinate cells and partially overlaps with *ROUGH SHEATH1* and *OUTER CELL LAYER4* transcripts. Also, in the inflorescence, *PLA1* transcript is localized in cells subtending the lateral primordia or bordering the newly established meristematic region, suggesting a more general role of *PLA1* in signaling between indeterminate and determinate cells during the formation of lateral organs. Spatial transcriptomics builds on RNA *in situ* hybridization, which assays relatively few transcripts at a time and provides a powerful complement to single cell transcriptomics that inherently removes cells from their native spatial context. Further improvements of resolution and sensitivity will greatly advance research in plant developmental biology.

## Introduction

Plants iteratively produce aerial organs throughout their lifespan at the shoot apex. Here, pluripotent stem cells in the shoot apical meristem (SAM) balance renewal of undifferentiated cells and founder cells fated for organogenesis (Sussex and Steeves, 1989). In maize, stem cell initials in the SAM tip divide at a slower rate relative to the more proliferative cell divisions where leaf primordia initiate, known as plastochron 0 (P0) (Satterlee et al., 2020). Concomitant with the downregulation of class I *KNOTTED1 (KN1)*-*LIKE HOMEODOMAIN (KNOX)* genes, the incipient leaf primordium (P0) develops a ring of cells forming the disc of insertion around the meristem in predictable alternate phyllotaxy (Hake et al., 1995). Together with the incipient leaf primordium, founder cells are recruited into an associated axillary meristem and subtending internode, forming a repeating phytomer unit of clonally related leaf, node, internode and axillary meristem (Sussex and Steeves, 1989). Newly emerged leaf primordia (~P4) display a transcriptomic prepatterning between proximal and distal regions (Leiboff et al., 2021); however, proximal-distal patterning of the ligule and auricle at the boundary between the distal blade and proximal sheath occurs in later primordia (~P6-P8) (Johnston et al., 2014).

Molecular signaling at the shoot apex crucially impacts plant architecture and, ultimately, yield (Kitagawa and Jackson, 2019). Understanding the spatiotemporal dynamics and relationships of gene co-expression patterns in the shoot apex is a key topic in plant biology. Decades of gene cloning and transcriptomics studies have identified a wealth of marker genes within the maize shoot apex. Functional genetic analyses have largely been complemented through RNA *in situ* hybridizations (ISH) to visualize spatiotemporal accumulation of RNA transcripts within tissues (Schneeberger et al., 1995; Hubbard et al., 2002; Gallavotti et al., 2004; Zhang et al., 2007; Knauer et al., 2019; Satterlee et al., 2020; Leiboff et al., 2021). Technologies, such as laser microdissection coupled with RNA sequencing (Brooks et al., 2009; Knauer et al., 2019) and single-cell RNA sequencing (Satterlee et al., 2020), that winnow organ- or tissue-level heterogeneity provide high-resolution transcriptomics. However, such approaches, where spatial context is lost, do not provide a *bona fide* characterization of hundreds of transcripts *in situ* in cells and tissues. Spatial transcriptomics is a revolutionary approach that provides a comprehensive understanding of hundreds of gene expression in tissues by retaining positional context within the tissue (Moor and Itzkovitz, 2017).

Spatial transcriptomics in animal studies have demonstrated that hundreds of gene expression profiles can be simultaneously visualized within the same tissue section, an advancement that has allowed the development of novel methods to analyze gene expression patterns and perform co-expression analyses (Vickovic et al., 2019; Chen et al., 2020). *In situ* sequencing (ISS) technology (Ke et al., 2013) was used to generate spatial maps of molecularly defined cell types in distinct tissue types as part of the international human cell atlas initiative (Sountoulidis et al., 2020; Wilbrey-Clark et al., 2020).

In animal tissues, the ISS technology was mainly applied on cryosections and multiplexed up to 86 genes (Ke et al., 2013; Chen et al., 2020). Briefly, for each gene, specific padlock probes are designed, each containing two arms that hybridize to the mRNA, an anchor sequence that allows visualization of all amplified probes, and a 6-bp gene-specific barcode. After hybridization, a ligation step circularizes the hybridized probes, which are subsequently amplified using rolling circle amplification, generating sub-micrometer sized DNA molecules. After amplification, a quality control step is performed by visualization of the amplified counts by hybridization of labeled anchor probes, which target each count, irrespective of gene target. Next, barcodes are decoded through sequencing by hybridization using an epifluorescence microscope and a 40x objective over six rounds of multicolor imaging. Finally, the sequenced counts are computationally decoded into the corresponding sequence, and gene-calling is performed for each count (Ke et al., 2013).

In plants, the few spatial transcriptomics studies published so far (Bowling et al., 2014; Giacomello et al., 2017; Giolai et al., 2019) show promise and feasibility to implement the technologies while highlighting room for its advancement with respect to multiplexing, resolution and sensitivity. Here, we leveraged ISS technology to colocalize the transcripts of 90 genes within tissue sections through the maize shoot apex. Our optimization steps included the use of formalin fixed and paraffin embedded (FFPE) tissue and cell segmentation. The resulting spatial map of the maize shoot apex illustrates that the ISS technology is highly suited to visualize expression patterns simultaneously for many genes and provides information about co-expression in specific cell types. In a case study, we used spatial co-expression data to infer a novel role for *PLASTOCHRON1 (PLA1)* as a gene that may function to delineate a boundary between indeterminate and determinate cells in meristems.

## Results and discussion

### Optimization of the ISS technology to analyze simultaneous gene expression in plant tissue

ISS is performed using fluorescence microscopy to image four different fluorescent labels (Alexa Fluor® 488, Cy3, Cy5 and Alexa Fluor® 750). We first evaluated whether the routinely used FFPE sections of plant tissue ~~displayed~~ could provide signal above auto-fluorescence in different channels. Paraffin was removed from FFPE sections using HistoClear, which was subsequently removed through an EtOH gradient and finally the sections were brought into an aqueous environment. We analyzed whether signal above background fluorescence was observed in the DAPI channel (emission at 450 nm) by staining WT shoot apices with DAPI (**Supplemental Figure S1A-C**), and in the RFP channel (emission at 584 nm) by evaluating RFP signal in harvested *DR5::RFP* transgenic shoot apices (**Supplemental Figure S1D-F**). Clear and specific signals were observed in both channels, indicating that autofluorescence did not interfere (**Supplemental Figure S1**). Previously, a distinct YFP signal (emission 504 to 526 nm) was shown in the maize SAM that was embedded and rehydrated in a similar way (Johnston et al., 2015). Because no obvious background signal was observed in the three channels (DAPI, YFP and RFP), we concluded that a clear signal could be observed across the majority of the visible spectrum, so we proceeded with FFPE sections to evaluate ISS chemistry in plant tissues. Maize samples were processed as described previously for regular ISH experiments (Zöllner et al., 2021), except for the omission of acetylation steps using tri-ethanolamine and acetic anhydride, which decreased the amplification efficiency.

To evaluate ISS and the simultaneous visualization of a panel of transcripts, we selected 90 genes (**Supplemental Table S1**) by cross-referencing in-house and published ISH patterns with tissue-specific expression levels obtained by laser microdissection of regions of the shoot apex (Brooks et al. 2009; Knauer et al. 2019). This approach allowed us to hone in on selected genes across a broad range of ~~cell types~~ functional domains and developmental zones to analyze the performance of the ISS technology in plant tissue (**Supplemental Table S1**).

Probes targeting transcripts of the entire 90 gene-panel were used for a pilot ISS experiment, where all 90 genes were amplified simultaneously and decoded on two consecutive longitudinal sections through the maize shoot apex. As quality-control, the anchor probe was used to visualize all amplified counts and overlaid with the DAPI staining, indicating that counts could be obtained in every tissue-type (**Supplemental Figure S2A-D**). During the sequencing, it was observed that tissue adhesion decreased during repeated washing steps and ISS, resulting in loss of tissue and failure to complete the sequencing. Therefore, we adapted the protocol to include a step (2 hours at 60°C) to bake the FFPE sections to the slide prior deparaffinization and a step (30 minutes at 37°C) prior mounting the

sections after the amplification steps. The addition of these two baking periods increased tissue-adhesion, allowing successful sequencing and visualization of expression profiles in maize shoot apex (**Figure 1A, Supplemental Figure S2D**). With the implementation of the optimized protocol, we observed highly specific expression patterns, as exemplified in meristem indeterminate cells (**Figure 1B, Supplemental Figure S3A**), leaf epidermis (**Figure 1C**), mesophyll (**Supplemental Figure S3F**), vasculature (**Figure 1D**), the central zone of the meristem (**Figure 1E, Supplemental Figure S3C**), lateral organ boundaries (**Supplemental Figure S3G**) and proximal cells of leaf primordia (**Supplemental Figure S3 B, D, E, H**). Additionally, we utilized ISS to array multiple gene expression profiles simultaneously within specific cells (**Figure 1F**).

To map the gene expression to individual cells, cell segmentation in the animal field is typically done by staining with DAPI (Ke et al., 2013). However, the various shapes of plant cells and the presence of the vacuole often de-centralizes the nucleus, necessitating the use of a cell wall stain, Calcofluor-white. Cell segmentation with CellPose (Stringer et al., 2021), combined with manual curation allowed successful segmentation for the majority of cell types, except for the vascular bundles (**Supplemental Figure 4A-B**). Retraining the deep learning-based segmentation algorithm CellPose (Stringer et al., 2021) using manually segmented vascular cells could improve segmentation of vascular bundles, allowing automated segmentation of entire shoot apices and rendering the segmentation more generic.

### **Validation of the ISS technology in plants**

With the optimized protocol from the pilot study, the 90 gene-panel was repeated on consecutive transverse and longitudinal sections throughout the maize apex. In a first step, the reproducibility of the ISS technology was evaluated between consecutive sections through the same shoot apex and between sections of independently embedded shoot apices of the same age. To ensure we were comparing concordant tissue, especially in independent sections, we made sure all images contained similar proportion of stem or leaf tissue, in addition to the SAM, by making sure the triangle between the SAM tip and the base of P2 and P3 was centered in the image. For each replicate, we compared the best section through the SAM, one section before and one section after. In these images, we normalized the count number for every gene, relative to the total number of counts and determined the  $R^2$  between the different sections. The correlation between consecutive sections was significant with an  $R^2$  between 0.99 and 0.55 ( $p \leq 0.01$ ), while the  $R^2$  between sections through independent SAMs ranged from 0.93 and 0.28, but was still significant ( $p \leq 0.01$ ; Supplemental Figure S5). The lower correlation could be due to the fact that there was more than one cell layer between the sections or that the cell layers were not completely aligned and different genes were either expressed or switched off. In addition, the expression profiles were highly similar over the different replicates, as exemplified for *PLA1*, where interpretation of the expression domain could depend on the sectioning angle (Supplemental Figure S6). Overall, the ISS technology resulted in comparable data between replicates.

Next, we analyzed whether the observed expression profiles by ISS corresponded to ISH. For 63 of the 90 genes, expression profiles were already published, or available in-house. 86.9% of successful probes in our ISS experiment genes corresponded to expression patterns of published and in-house single gene ISH (**Supplemental Table S1; Figure 2; Supplemental Figure S7**). In addition, the ISS profiles of 17 genes with a range of expression levels (Knauer et al. 2019) in the shoot apex were successfully obtained: *PIN-FORMED1a* (*PIN1a*; **Figure 2A-B**), *ANGUSTIFOLIA3* (*AN3*; **Figure 2C-D**), *GROWTH REGULATING FACTOR1* (*GRF1*; **Figure 2E-F**); *CUP-SHAPED COTELYDON2* (*CUC2*; **Figure 2G-H**), *BIG EMBRYO1* (*BE1*; **Figure 2I-J**), *LIKE AUXIN RESISTANT2* (*LAX2*; **Figure 2K-L**), *DYNAMIN RELATED*

*PROTEIN4a* (*ZmDRP4a*; **Figure 2M-N**) and *HISTONE4* (*H4*; **Figure 2O-P**), marking more general (*Histone H4*; **Figure 2O-P**) or highly specific expression profiles (*CUC2*; **Figure 2G-H**).

After segmentation, gene expression was mapped to each individual cell and the distribution of counts, for all 90 genes, per cell was analyzed (Supplemental Figure S8). The distribution of counts per cell was skewed towards a low number of total gene counts per cell, where 72.1% of cells contain between 0-9 expression counts, and less than 10% of cells contain more than 20 counts per cell. To illustrate that the resolution can be brought to single cell level, we show the expression profile of *H4*, a marker for cell division, in dividing cells in the shoot apex (Supplemental Figure S9). Counts depicting *H4* expression (Supplemental Figure S9A) can be identified at the level of single cells (Supplemental Figure S9B), which are well defined when combining DAPI with cell wall stains (Supplemental Figure S9C). These data indicate that the resolution of the ISS technology can potentially be used to evaluate gene expression at single cell level.

For some genes, such as *KN1*, the expression profile obtained by ISS was fainter and present in fewer cells than based on the ISH (Supplemental Figure 3A; Supplemental Figure S7O-P). It was described that generation of rolling circle amplification products during the amplification step could reduce sensitivity by optical crowding (Strell et al., 2019). Therefore, we evaluated whether optical crowding could reduce signal by comparing expression of *CUC2* in an experiment with three probes (*PLA1*, *CUC2* and *DRL1*; Supplemental Figure S10A) and the full gene panel experiment (Supplemental Figure S10B). Although both experiments show *CUC2* expression at the organ boundaries, it is evident that there is a loss of sensitivity when analyzing 90-genes simultaneously (Supplemental Figure S10A-B). The rolling circle amplification of many probes in a single cell, thus, most likely resulted in challenges during the computational decoding of signals, leading to loss of signal.

For 15 genes out of the 90, a range from no expression to 15 counts was observed and were considered stochastic (e.g. *2G488001*; *WUSCHEL1*; *WUSCHEL2*; *ORPHAN337ortholog*; *PIN1d*; *WUSCHEL-RELATED HOMEBOX9B* (*WOX9B*); *WOX9C*; *INDETERMINATE1*; *DROOPING LEAF1* (*DRL1*), *HIGH AFFINITY K+ TRANSPORTER5* (*HAK5*), *RAMOSA3* (*RA3*), *TERMINAL EAR-LIKE1* (*TEL1*), *FON2-LIKE CLE PROTEIN1* (*FCP1*), *maize ZEA MAYS MADS4* (*ZMM4*) and *ABPHYL1*). The expression patterns of these genes were previously shown across different tissue-types, such as the meristem (Satterlee et al., 2020), leaf primordia (Lee et al., 2009a), leaves (Danilevskaya et al., 2008b; Strable et al., 2017), and vascular bundles (Qin et al., 2019). In addition, *DRL1* expression was also not observed in the three-probe experiment (data not shown), indicating that the inability to detect them likely was not due to possible optical crowding of signal in a specific tissue-type. In addition, we could not find a correlation between detecting expression of a gene via ISS and its expression level as determined via laser microdissection coupled with RNA sequencing (**Supplemental Table S1**). Therefore, the most likely reason these genes were unsuccessful lies in the probe design or technical artefacts.

### **Spatial transcriptome map of the maize shoot apex**

To evaluate the specificity of the ISS technology, we looked in greater detail to the obtained expression profiles in the different tissue types of the maize shoot apex. The expression domains of *ARGONAUTE18a* (Knauer et al., 2019) (*AGO18a*), *DRP4a* (Knauer et al., 2019) and *LONELY GUY7* (Knauer et al., 2019a) (*LOG7*) mark the SAM tip, while *YABBY9* (Juarez et al., 2004) (*YAB9*) and *YAB14* (Juarez et al., 2004) are expressed in incipient leaf primordia (**Figure 3A**). Early expression of maize *CUC2* (Johnston et al., 2014), *CUC3* (Knauer et al., 2019), and *DWARF11-LIKE* (Johnston et al., 2014) (*D11-LIKE*) demarcates a boundary region between leaf primordia and the SAM. Further elaboration of the phytomer is governed by *BARREN STALK1* (Gallavotti et al., 2004) (*BA1*) and *BARREN STALK FASTIGIATE1* (Gallavotti et al., 2011) (*BAF1*) that mark the boundary of the axillary meristem. *TEOSINTE*

*BRANCHED1* (Hubbard et al., 2002) (*TB1*) and its direct target *GRASSY TILLERS1* (Whipple et al., 2011) (Dong et al., 2019) (*GT1*) are co-expressed in the axillary meristem (**Figure 3B-C, Supplemental Figure S11A**). *OUTER CELL LAYER4* (Vernoud et al., 2009) (*OCL4*) transcripts accumulate in the L1 layer and epidermis, while expression of *MILKWEED POD1* (*MWP1*) (Candela et al., 2008) encoding a KANADI protein, accumulates in the abaxial epidermis. Additional leaf polarity marker genes, *AUXIN RESPONSE FACTOR3a* (Johnston et al., 2014) (*ARF3a*) and *ROLLED LEAF1* (Juarez et al., 2004) (*RLD1*) are expressed in the abaxial epidermis and abaxial subepidermal cells of primordia, respectively, as well as in vascular cells. Mesophyll cells are marked by *JACALIN-RELATED-LECTIN* (*JRL*) transcripts (Zhang et al., 2007) (**Supplemental Figure S11B-D**).

Besides *ARF3a* and *RLD1*, several other genes are expressed in developmental sequence in vascular cells. Maize *PIN1a* (Gallavotti et al., 2008), encoding an auxin transporter, and *BARREN INFLORESCENCE1* (ISS data), encoding an *AUXIN/INDOLE-3-ACETIC ACID* (*Aux/IAA*) transcripts mark the core SAM and in the vasculature of developing primordia. Maize *GLUTAREDOXIN-C8* (Yang et al., 2015; Knauer et al., 2019) (*GRXC8*) and *ARF3a* (Johnston et al., 2014) transcripts do not appear in the SAM but are detected in the P0 primordium. Maize genes *LAX2* (Leiboff et al., 2015), encoding an auxin influx protein, and *ZEA CENTRORADIALIS1/3* (Danilevskaya et al., 2008) (*ZCN1/3*) are expressed in the vasculature from P2 onward, while *NICOTIANAMINE SYNTHASE3* (Zhou et al., 2013) (*NAS3*) is expressed in the vasculature of later primordia (**Figure 3C**).

We have established a webtool where researchers can select and visualize various combinations of gene expression patterns to construct a spatial expression atlas of the maize shoot apex <https://bioinformatics.psb.ugent.be/webtools/spatial-transcriptomics/index.php>.

### ***PLASTOCHRON1* is expressed at the boundary between undifferentiated and differentiated cells**

We further utilized spatial transcriptomics to understand the spatiotemporal dynamics of *PLASTOCHRON1* (*PLA1*) expression in the maize shoot apex. *PLA1*, a member of the *CYTOCHROME P450 78A* (*CYP78A*) gene family, crucially regulates organ growth by controlling the duration of cells ability to divide (Sun et al., 2017). Because the transposon insertion for the published *pla1-1* allele was at a splice site (Sun et al., 2017), it was uncertain whether it could be considered a knock-out, so we generated an additional allele using genome editing in B104. The *pla1-2* allele was obtained by a dual guide RNA approach, both targeted against the first exon. The fragment between both predicted cut sites was excised, inverted and reintegrated, resulting in a premature stop codon. The homozygous *pla1-2* mutants (Supplemental Figure S12 A) displayed a significantly decreased plastochron, resulting in the generation of more leaves compared to the WT in the same time-period (Supplemental Figure S12C) and a reduced leaf length (Supplemental Figure S12B), which was due to a slight decrease of leaf elongation rate (LER) and a strong decrease in leaf elongation duration (LED), visualized by the early decline in LER (Supplemental Figure S12D). Overall, the observed phenotypes of both alleles were very similar and pointed towards a role of *PLA1* in timing of leaf initiation and growth.

To our knowledge, neither the role of *PLA1* nor the *in situ* accumulation of its transcripts have been described in the maize shoot apex. *PLA1* is a putative direct target of *KN1* (Bolduc et al., 2012), and is co-expressed with the Class I *KNOX* genes *KN1* and *RS1*, and 170 other putative direct *KN1* target genes (Leiboff et al., 2021) that are highly expressed in indeterminate cells that presumably reside in the SAM and at the base of young primordia (Satterlee et al., 2020; Leiboff et al., 2021).

*PLA1* is expressed in a spiral ring around the SAM, and similar to class I *KNOX* expression, is absent from P0 cells (**Figure 4A-D**). *PLA1* transcripts were not detected in the central zone of the SAM, nor in

fully-emerged leaf primordia; rather, the *PLA1* expression domain subtends leaf primordia mainly along the abaxial side. Quantification of the *PLA1* expression per cell highlights maximal *PLA1* expression in regions subtending leaf primordia and lower expression in the spiral between two consecutive primordia (**Figure 4E**). *PLA1* transcript accumulation at the base of primordia importantly impacts overall leaf growth (Sun et al., 2017; Supplemental Figure S12B) because *PLA1* expression progressively decreases across older plastochrons. Additionally, *PLA1* expression is greater at the base of the leaves in a *GA2ox::PLA1* line (Sun et al., 2017), resulting in longer leaf growth (**Figure 4F**).

The spiral transcriptomic profile of *PLA1* mirrored that of *RS1* (Schneeberger et al., 1995); however, *PLA1* and *RS1* expression domains do not entirely overlap, as *PLA1* is not expressed throughout the ribzone of the SAM, where *RS1* transcripts accumulate (**Figure 5A**). However, there is a sharp demarcation (**Figure 5C**) of indeterminate cells, marked by *RS1* expression (**Figure 5A**) and determinate cells, as is visualized by *OCL4* expression (**Figure 5B**). The expression of *PLA1* is exactly at the boundary between the indeterminate and determinate cells and partially overlaps with both *RS1* and *OCL4* (**Figure 5D-E**). These data suggest that *PLA1* functions at the boundary between indeterminate cells within the SAM and cells in the incipient leaf primordium where it imposes indeterminacy, which is in accordance with its role in leaf growth (Sun et al., 2017; Supplemental Figure S12D).

We utilized ISS to explore the hypothesis that *PLA1* defines a boundary of indeterminate cells in a region between the peripheral meristem and proximal leaf primordium, which is necessary to drive proper differentiation and growth processes. The expression of *PLA1* in these putative indeterminate cells was validated in the inflorescence, which provides numerous opportunities to observe boundaries between meristems and lateral primordia. Ear spikelet meristems and floret meristems express *PLA1* in a ring of cells adjacent to lateral primordia, and, in the case of floret meristems, the newly established meristematic region (**Supplemental Figure S13A-B**). Similar to *PLA1* regulating leaf length, these data are consistent with the increased ear length and subsequent yield when *PLA1* is ectopically expressed (Sun et al., 2017), suggesting a broader role for *PLA1* in signaling between indeterminate meristematic cells and determinate cells in lateral organs. Supporting this hypothesis are the complementary expression patterns between *PLA1* and *KN1* (**Supplementary Figure S13C**), marking indeterminate cells, and *YAB15* (**Supplemental Figure S13D**) expressed in differentiated lateral primordia. Collectively, these data suggest that *PLA1* marks, or pre-patterns, boundaries between indeterminate cells and determinate lateral organ primordia.

With *PLA1* marking a boundary between indeterminate and determinate cells, we leveraged ISS to compare simultaneously the *in situ* transcript profiles of *PLA1* to *CUC2* and *D11-LIKE* boundary genes. Overlaying *PLA1* and *CUC2* arrays in the maize shoot apex revealed that their expression domains are mutually exclusive. *PLA1* transcripts are absent from founder cells that are enriched in the co-expressed *CUC2* and *D11-LIKE* genes, which mark the disc of insertion (Johnston et al., 2014; Johnston et al., 2015) (**Figure 6A**), and, interestingly, that also overlap with *BA1* in younger leaf primordia, and with *BAF1* transcripts in older primordia (**Figure 6B**). While *PLA1* does not appear to be expressed in the disc of insertion, its transcripts accumulate in a ring-like pattern around the stem in cells that co-express *AN3* (**Figure 6C**). Intriguingly, the ring-like patterns of *D11-LIKE* expression are in cells that subtend *PLA1* and *AN3* domains (**Figure 6D**). Collectively, the data provide new spatial context for *PLA1* together with co-expressed genes at the base of the developing organs within regions that are established by key regulators of organ boundaries. This is in accordance with previous findings in Arabidopsis where *KLUH*, a homolog of *PLA1*, functions downstream of *CUC2* (Maugarny-Calès et al., 2019).

We found that *PLA1* transcripts do not accumulate in the SAM tip, which is marked by high expression of *LOG7*, a cytokinin-activating enzyme (Chickarmane et al., 2012). Furthermore, *PLA1* is not detected

in primordia that typically have high auxin levels, nor in boundary cells typified by low levels of auxin and brassinosteroids (Johnston et al., 2014; Maugarny-Calès and Laufs, 2018). The simultaneous projection of *PLA1* and *PIN1a* expression in the maize shoot apex shows that *PLA1* and *PIN1a* expression domains are mutually exclusive (**Figure 6E**). Together, these data indicate that *PLA1* is not expressed in cells with high levels of auxin or cytokinin. Perturbations of *CYP78A* genes in eudicot and monocot species alters cytokinin and auxin levels (Sun et al., 2017; Jiang et al., 2021). The balance between the two hormones is crucial to meristem activity (Schaller et al., 2015), controlling phyllotaxy and plastochron index (Lee et al., 2009b; Besnard et al., 2014), and organ size (Zhu et al., 2020), suggesting that *PLA1* could act under control of auxin and cytokinin or affects their activity.

## Conclusions

We modified the ISS spatial transcriptomics technology (Ke et al., 2013) so it can routinely be used in plant tissues. We applied the ISS technology in the maize shoot apex and quantified mRNAs of numerous genes simultaneously within cells while preserving spatial relationships within tissues. Not only was the technology used on FFPE sections, but we also improved tissue adherence and added a cell wall stain to aid plant cell segmentation. The ISS technology was significantly reproducible between consecutive and independent sections. For some genes, a stochastic signal was obtained that could not be correlated to the pattern of transcripts detected through ISH. Although the gene panel contained some genes for which expression was previously shown in inflorescence meristems and expression in the shoot apex could be absent, for the majority of the genes, the lower success rate was most likely due to probe design or technical issues. For the genes that showed sufficient counts, the vast majority (88.5%) of the expression profiles correlated to those observed by ISH. Optical crowding (Strell et al., 2019) was one possible explanation for expression profiles that were less pronounced or intense than what was observed by ISH. Also, there are some inherent differences between ISH and ISS, because in ISS all 90 probes were combined and hybridized in one library and were only sequenced in 5 cycles, while for ISH, probe concentration and exposure time is adjusted for each individual gene. Overall, we developed a pipeline from tissue embedding to cell segmentation that can be easily transferred between plant tissues and species.

The ISS technology provides a powerful tool to compare transcript accumulation of several genes simultaneously in a tissue context that can be up to one cm<sup>2</sup> and thus large tissue samples. However, in its current state, resolution and sensitivity of ISS does not allow robust cellular localization and quantification. These challenges will likely be addressed in the near future, as the field of spatial transcriptomics is rapidly evolving and different technology platforms, in addition to ISS, are developed (Eng et al., 2019; Rodrigues Samuel et al., 2019; Vickovic et al., 2019; Stickels et al., 2020). We believe that the optimizations we present here bring the ISS technology to plants and will also be applicable to other spatial transcriptomics technologies, opening an entire array of spatial technologies in plants.

Gradients, the directional flow of molecules and a temporal chain of events, can determine microenvironments within one tissue. Such spatial heterogeneity is reflected by the molecular identity of the distinct cell types and/or cellular domains, and is often lost in bulk RNA sequencing experiments and is frequently studied in developmental plant biology by single gene ISH. Our results complement and expand upon transcript accumulation patterns reported previously by single gene ISH, as well as high-resolution transcriptomics afforded by laser microdissection coupled with RNA sequencing (Knauer et al. 2019) and single cell RNA-sequencing studies (Satterlee et al., 2020). Single cell RNA-sequencing approaches offer unprecedented opportunities to distinguish cellular subpopulations and tissue domains, but these techniques require tissue dissociation and, thus, lose the spatial

coordinates of the cells. Spatial transcriptomics will likely become a technology that will be performed side-by-side with single cell RNA-sequencing studies to validate the spatial context of the top genes identified per cell cluster. Because spatial transcriptomics approaches need sequence information but no transformation to generate marker lines to confirm single cell RNA-sequencing, it will be widely applicable to many plant species (Seyfferth et al., 2021). As such, spatial transcriptomics will provide valuable information on the dynamics of expression domains in many developmental settings, by comparing genetic perturbations, natural variation or commercial varieties, and upon abiotic and biotic interactions.

Because the maize shoot apex is comprised of meristem, primordia and associated phytomer that inherently represent gradual developmental stages, we captured the concurrent temporal sequence of transcriptional events within a spatial context for numerous genes. By leveraging spatial transcriptomics, we identified putative roles for *PLA1* in imposing indeterminate cell fate and in balancing the actions of auxin and cytokinin. The *PLA1* expression at the boundary between determinate and indeterminate cells were confirmed in the inflorescence meristem, rendering *PLA1* a more general regulator of lateral organ formation. This role of *PLA1* was also deduced from the *pla1-1* (Sun et al., 2017) and the *pla1-2* allele that displayed more leaves that were affected in the time during which the cells maintained division capacity. Future research is needed to expand the network around *PLA1* and position it relative to known players that function in cell determinacy programs.

## Material and Methods

### Accession numbers

*PLA1* GRMZM2G167986

### Plant materials, growth conditions and phenotyping

Maize B104 and *GA2ox::PLA1* (in B104 background; Sun et al., 2017) seedlings were grown under growth chamber conditions with controlled relative humidity (55%), temperature (24 °C day/18 °C night), and light intensity (170–200 μmol per m<sup>2</sup> per second photosynthetic active radiation at plant level) provided by a combination of high-pressure sodium vapour (RNP-T/LR/400W/S/230/E40; Radium) and metal halide lamps with quartz burners (HRI-BT/400W/D230/E40; Radium) in a 16 h/8 h (day/night) cycle.

The *pla1-2* allele was generated by designing two guides (guide 1: AAAGATCAGGCCAGCCAGGAGGG; guide 2: AGACCACGGGGTCCCACGATAGG) against the first exon. Both guides were assembled into the pBUN411 vector by first incorporating them in a pCBC-MT1T2 vector-fragment through PCR, followed by PCR-purification. Next purified PCR-fragments were assembled in pBUN411 through golden gate cloning as described in (Pedroza-Garcia et al., 2021). The vector was sequence validated and transformed into *Agrobacterium tumefaciens*, which was used to transform immature maize embryos (Coussens et al., 2012). Primers used for cloning and genotyping are listed in **Supplemental Table 2**. Leaf number was counted over plant development and leaf 4 length was measured daily during the growth period to determine final leaf length, growth rate and growth duration.

### Tissue collection, embedding and sectioning for spatial transcriptomics and regular ISH

Ten days post germination B104 seedlings were harvested to collect shoot apex samples for *in situ* hybridizations and *in situ* sequencing and *GA2ox::PLA1* samples of the same age were used for *in situ* hybridizations. Greenhouse grown B104 ears and field grown B73 ears were harvested for *in situ*

hybridization when they reached a length of approximately 10 mm. Samples were fixed at 4 degrees in 4% PFA, pulled vacuum until complete penetration of the tissue and stored overnight at 4 degrees. Fixed samples were dehydrated through a gradient to 100% EtOH at 4 degrees, cleared using HistoClear through an EtOH/HistoClear gradient until 100% HistoClear is reached at room temperature, next paraplast chips are added to the samples at 100% HistoClear and allowed to partially dissolve overnight. The samples are then placed in an oven at 60 degrees, allowing complete dissolution of the paraplast chips. Once chips are dissolved, the HistoClear is replaced by liquid paraplast which was changed twice a day over the course of three days to ensure complete penetration of the tissue with paraplast. Next the samples were embedded using a tissue embedding center (HistoCenter). Embedded samples were finally sectioned in 7µm thick sections using a microtome (Reichert-Jung 2040).

### **mRNA *in situ* hybridization protocol**

Tissues were harvested and processed as described above. ISH protocol was performed as described by (Zöllner et al., 2021). Mounted slides were imaged using an Olympus BX51 light microscope. Primers used for probe generation are listed in Supplemental Table 2. ISH were repeated at least twice.

### **Spatial transcriptomics: section preparation and probe hybridization, ligation, amplification and visualization**

In total, three biological repeats were obtained for the longitudinal sections of the SAM. Two consecutive sections were included in the pilot experiment and imaged at 20X magnification. For the actual experiment we included two biological repeats, each consisting of nine consecutive sections, which were imaged at 40X magnification. For the transverse section, a single biological repeat consisting of sixteen consecutive sections was used, which were imaged at 40X magnification. Both longitudinal and transverse sections were processed identically.

Paraffin embedded sections were baked to the slides for 2 hours at 60 degrees, the paraffin was partially melted but tissues adhered to the slides. Next, the sections were deparaffinized by two 30 minutes 100% HistoClear steps. A gradient was applied to remove the HistoClear and replace it with EtOH, with 1 minute per step. Finally, sections were brought in an aqueous solution by removing EtOH through a gradient, again each step 1 minute. Rehydrated sections received a proteinase treatment (Pronase: Sigma Aldrich) for 15 minutes which was stopped by placing sections in 0.2% glycine dissolved in PBS. Sections were dehydrated through a gradient to 100% EtOH conditions.

For library preparation, the for a panel of 90 genes were hybridized overnight at 37°C, then ligated before the rolling circle amplification was performed overnight at 30°C using the HS Library Preparation kit for CARTANA technology and following manufacturer's instructions. To prevent tissue sections detachment, an additional baking step of 30 minutes at 37°C was performed before mounting. Exclusively Slow Fade Antifade Mountant, 10µL for one square cm, was used to mount sections. Quality control of the library preparation was performed by applying anchor probes to detect simultaneously all rolling circle amplification products from the panel. Anchor probes are labeled probes with Cy5 fluorophore (excitation at 650nm and emission at 670nm). All samples passed the QC and were sent to CARTANA Sweden (part of 10xGenomics), for *in situ* barcode sequencing, imaging and data processing. Briefly, adapter probes and sequencing pools (containing 4 different fluorescent labels: Alexa Fluor® 488, Cy3, Cy5 and Alexa Fluor® 750) were hybridized to the padlock probes to detect the gene-specific barcodes, through a sequence specific signal for each gene specific rolling circle amplification product. This was followed by imaging and was performed 6 times in a row to allow for the decoding of all genes in the panel. Raw data consisting of 40x images from 5 fluorescent channels (DAPI, Alexa Fluor® 488, Cy3, Cy5 and Alexa Fluor® 750) were each taken as z-stack and flattened to

2D using maximum intensity projection. After image processing and decoding, the results are summarized in a csv file and gene plots are generated using MATLAB.

### Segmentation

The images obtained from the DAPI and Calcofluor-White stain were merged using bftools (<https://docs.openmicroscopy.org/bio-formats/5.7.1/users/comlinetools/index.html>). Due to the large image size, the merged image was transformed in a pyramid image, where resolution is decreased when fully zoomed out and incrementally increases when zooming in. A composite image was made of DAPI and Calcofluor White stains and imported in QuPATH V0.2.3 (Bankhead et al. 2017). Gene expression was converted to a QuPath point format to allow visualization of gene expression profiles. Next, the composite image was exported in tiles, and all tiles were segmented using CellPose (Stringer et al., 2021). Segmented cells were again imported into QuPath, and missing or badly annotated cells were manually curated. Overlapping cell boundaries were merged to ensure a single gene expression point could not be allocated to multiple cells. The segmented cells were saved as regions of interest (ROI), and gene expression points were allocated to segmented cells. The scripts for QuPATH and CellPose can be found in Supplemental dataset1.

### Acknowledgements

Tech Watch VIB funded the *in situ* sequencing; R. L. and J. J. were funded through FWO (pre-doc grant 1S10817N and bilateral project G0D8919N, respectively). The authors are very grateful to Malte Kuhnemund, Morgane Rouault and colleagues from CARTANA Sweden, 10x Genomics for their help to bring their technology to plants and to Michiel Van Bel who developed the online tool to visualize the data.

### References

- Besnard F, Refahi Y, Morin V, Marteaux B, Brunoud G, Chambrier P, Rozier F, Mirabet V, Legrand J, Lainé S, et al** (2014) Cytokinin signalling inhibitory fields provide robustness to phyllotaxis. *Nature* **505**: 417–421
- Bolduc N, Yilmaz A, Mejia-Guerra MK, Morohashi K, O'Connor D, Grotewold E, Hake S** (2012) Unraveling the KNOTTED1 regulatory network in maize meristems. *Genes Dev* **26**: 1685–1690
- Bowling AJ, Pence HE, Church JB** (2014) Application of a novel and automated branched DNA *in situ* hybridization method for the rapid and sensitive localization of mRNA molecules in plant tissues. *Appl Plant Sci*. doi: 10.3732/apps.1400011
- Brooks III L, Strable J, Zhang X, Ohtsu K, Zhou R, Sarkar A, Hargreaves S, Elshire RJ, Eudy D, Pawlowska T, et al** (2009b) Microdissection of Shoot Meristem Functional Domains. *PLOS Genet* **5**: e1000476
- Candela H, Johnston R, Gerhold A, Foster T, Hake S** (2008) The milkweed *pod1* gene encodes a KANADI protein that is required for abaxial/adaxial patterning in maize leaves. *Plant Cell* **20**: 2073–2087
- Chen W-T, Lu A, Craessaerts K, Pavie B, Sala Frigerio C, Corthout N, Qian X, Laláková J, Kühnemund M, Voytyuk I, et al** (2020) Spatial Transcriptomics and *In Situ* Sequencing to Study Alzheimer's Disease. *Cell* **182**: 976-991.e19
- Chickarmane VS, Gordon SP, Tarr PT, Heisler MG, Meyerowitz EM** (2012) Cytokinin signaling as a positional cue for patterning the apical-basal axis of the growing *Arabidopsis* shoot meristem.

- Coussens G, Aesaert S, Verelst W, Demeulenaere M, Buck S De, Njuguna E, Inzé D, Lijsebettens M Van** (2012) Brachypodium distachyon promoters as efficient building blocks for transgenic research in maize. *J Exp Bot* **63**: 4263–4273
- Danilevskaya ON, Meng X, Hou Z, Ananiev E V, Simmons CR** (2008a) A genomic and expression compendium of the expanded PEBP gene family from maize. *Plant Physiol* **146**: 250–264
- Danilevskaya ON, Meng X, Selinger DA, Deschamps S, Hermon P, Vansant G, Gupta R, Ananiev E V, Muszynski MG** (2008b) Involvement of the MADS-Box Gene ZMM4 in Floral Induction and Inflorescence Development in Maize . *Plant Physiol* **147**: 2054–2069
- Dong Z, Xiao Y, Govindarajulu R, Feil R, Siddoway ML, Nielsen T, Lunn JE, Hawkins J, Whipple C, Chuck G** (2019) The regulatory landscape of a core maize domestication module controlling bud dormancy and growth repression. *Nat Commun* **10**: 3810
- Eng C-HL, Lawson M, Zhu Q, Dries R, Koulena N, Takei Y, Yun J, Cronin C, Karp C, Yuan G-C, et al** (2019) Transcriptome-scale super-resolved imaging in tissues by RNA seqFISH+. *Nature* **568**: 235–239
- Gallavotti A, Malcomber S, Gaines C, Stanfield S, Whipple C, Kellogg E, Schmidt RJ** (2011) BARREN STALK FASTIGIATE1 is an AT-hook protein required for the formation of maize ears. *Plant Cell* **23**: 1756–1771
- Gallavotti A, Yang Y, Schmidt RJ, Jackson D** (2008) The Relationship between auxin transport and maize branching. *Plant Physiol* **147**: 1913–1923
- Gallavotti A, Zhao Q, Kyojuka J, Meeley RB, Ritter MK, Doebley JF, Enrico Pè M, Schmidt RJ** (2004) The role of barren stalk1 in the architecture of maize. *Nature* **432**: 630–635
- Galli M, Liu Q, Moss BL, Malcomber S, Li W, Gaines C, Federici S, Roshkovan J, Meeley R, Nemhauser JL, et al** (2015) Auxin signaling modules regulate maize inflorescence architecture. *Proc Natl Acad Sci U S A* **112**: 13372–13377
- Giacomello S, Salmén F, Terebieniec BK, Vickovic S, Navarro JF, Alexeyenko A, Reimegård J, McKee LS, Mannapperuma C, Bulone V, et al** (2017) Spatially resolved transcriptome profiling in model plant species. *Nat plants* **3**: 17061
- Giolai M, Verweij W, Lister A, Heavens D, Macaulay I, Clark MD** (2019) Spatially resolved transcriptomics reveals plant host responses to pathogens. *Plant Methods* **15**: 114
- Hake S, Char BR, Chuck G, Foster T, Long J, Jackson D** (1995) Homeobox genes in the functioning of plant meristems. *Philos Trans R Soc London Ser B, Biol Sci* **350**: 45–51
- Hubbard L, McSteen P, Doebley J, Hake S** (2002) Expression patterns and mutant phenotype of teosinte branched1 correlate with growth suppression in maize and teosinte. *Genetics* **162**: 1927–1935
- Jiang L, Yoshida T, Stiegert S, Jing Y, Alseekh S, Lenhard M, Pérez-Alfocea F, Fernie AR** (2021) Multi-omics approach reveals the contribution of KLU to leaf longevity and drought tolerance. *Plant Physiol* **185**: 352–368
- Johnston R, Leiboff S, Scanlon MJ** (2015) Ontogeny of the sheathing leaf base in maize (*Zea mays*). *New Phytol* **205**: 306–315
- Johnston R, Wang M, Sun Q, Sylvester AW, Hake S, Scanlon MJ** (2014) Transcriptomic Analyses Indicate That Maize Ligule Development Recapitulates Gene Expression Patterns That Occur

during Lateral Organ Initiation . *Plant Cell* **26**: 4718–4732

**Juarez MT, Twigg RW, Timmermans MCP** (2004) Specification of adaxial cell fate during maize leaf development. *Development* **131**: 4533–4544

**Ke R, Mignardi M, Pacureanu A, Svedlund J, Botling J, Wählby C, Nilsson M** (2013) In situ sequencing for RNA analysis in preserved tissue and cells. *Nat Methods* **10**: 857–860

**Kitagawa M, Jackson D** (2019) Control of Meristem Size. *Annu Rev Plant Biol* **70**: 269–291

**Knauer S, Javelle M, Li L, Li X, Ma X, Wimalanathan K, Kumari S, Johnston R, Leiboff S, Meeley R, et al** (2019c) A high-resolution gene expression atlas links dedicated meristem genes to key architectural traits. *Genome Res* **29**: 1962–1973

**Lee B, Johnston R, Yang Y, Gallavotti A, Kojima M, Travençolo BAN, Costa L da F, Sakakibara H, Jackson D** (2009a) Studies of aberrant phyllotaxy1 Mutants of Maize Indicate Complex Interactions between Auxin and Cytokinin Signaling in the Shoot Apical Meristem . *Plant Physiol* **150**: 205–216

**Lee B, Yu S, Jackson D** (2009b) Control of Plant Architecture: The Role of Phyllotaxy and Plastochron. *J Plant Biol* **52**: 277–282

**Leiboff S, Li X, Hu H-C, Todt N, Yang J, Li X, Yu X, Muehlbauer GJ, Timmermans MCP, Yu J, et al** (2015) Genetic control of morphometric diversity in the maize shoot apical meristem. *Nat Commun* **6**: 8974

**Leiboff S, Strable J, Johnston R, Federici S, Sylvester AW, Scanlon MJ** (2021) Network analyses identify a transcriptomic proximodistal prepatterning in the maize leaf primordium. *New Phytol* **230**: 218–227

**Maugarny-Calès A, Cortizo M, Adroher B, Borrega N, Gonçalves B, Brunoud G, Vernoux T, Arnaud N, Laufs P** (2019) Dissecting the pathways coordinating patterning and growth by plant boundary domains. *PLoS Genet* **15**: e1007913–e1007913

**Maugarny-Calès A, Laufs P** (2018) Getting leaves into shape: a molecular, cellular, environmental and evolutionary view. *Development*. doi: 10.1242/dev.161646

**Moor AE, Itzkovitz S** (2017) Spatial transcriptomics: paving the way for tissue-level systems biology. *Curr Opin Biotechnol* **46**: 126–133

**Pedroza-Garcia JA, Eekhout T, Achon I, Nisa M-U, Coussens G, Vercauteren I, Van den Daele H, Pauwels L, Van Lijsebettens M, Raynaud C, et al** (2021) Maize ATR safeguards genome stability during kernel development to prevent early endosperm endocycle onset and cell death. *Plant Cell* **33**: 2662–2684

**Qin Y-J, Wu W-H, Wang Y** (2019) ZmHAK5 and ZmHAK1 function in K<sup>+</sup> uptake and distribution in maize under low K<sup>+</sup> conditions. *J Integr Plant Biol* **61**: 691–705

**Rodrigues Samuel, R. SR, Aleksandrina G, A. MC, Evan M, R. VC, Joshua W, M. CL, Fei C, Z. ME** (2019) Slide-seq: A scalable technology for measuring genome-wide expression at high spatial resolution. *Science* (80- ) **363**: 1463–1467

**Satterlee JW, Strable J, Scanlon MJ** (2020) Plant stem-cell organization and differentiation at single-cell resolution. *Proc Natl Acad Sci* **117**: 33689 LP – 33699

**Schaller GE, Bishopp A, Kieber JJ** (2015) The yin-yang of hormones: cytokinin and auxin interactions in plant development. *Plant Cell* **27**: 44–63

**Schneeberger RG, Becraft PW, Hake S, Freeling M** (1995) Ectopic expression of the knox homeo box

gene rough sheath1 alters cell fate in the maize leaf. *Genes Dev* **9**: 2292–2304

- Settles AM, Holding DR, Tan BC, Latshaw SP, Liu J, Suzuki M, Li L, O'Brien BA, Fajardo DS, Wroclawska E, et al** (2007) Sequence-indexed mutations in maize using the UniformMu transposon-tagging population. *BMC Genomics* **8**: 116
- Seyfferth C, Renema J, Wendrich JR, Eekhout T, Seurinck R, Vandamme N, Blob B, Saeys Y, Helariutta Y, Birnbaum KD, et al** (2021) Advances and Opportunities in Single-Cell Transcriptomics for Plant Research. *Annu Rev Plant Biol* **72**: 847–866
- Sountoulidis A, Liontos A, Nguyen HP, Firsova AB, Fysikopoulos A, Qian X, Seeger W, Sundström E, Nilsson M, Samakovlis C** (2020) SCRINSHOT enables spatial mapping of cell states in tissue sections with single-cell resolution. *PLOS Biol* **18**: e3000675
- Stickels RR, Murray E, Kumar P, Li J, Marshall JL, Di Bella D, Arlotta P, Macosko EZ, Chen F** (2020) Sensitive spatial genome wide expression profiling at cellular resolution. *bioRxiv* 2020.03.12.989806
- Strable J, Wallace JG, Unger-Wallace E, Briggs S, Bradbury PJ, Buckler ES, Vollbrecht E** (2017) Maize YABBY Genes drooping leaf1 and drooping leaf2 Regulate Plant Architecture. *Plant Cell* **29**: 1622–1641
- Strell C, Hilscher MM, Laxman N, Svedlund J, Wu C, Yokota C, Nilsson M** (2019) Placing RNA in context and space – methods for spatially resolved transcriptomics. *FEBS J* **286**: 1468–1481
- Stringer C, Wang T, Michaelos M, Pachitariu M** (2021) Cellpose: a generalist algorithm for cellular segmentation. *Nat Methods* **18**: 100–106
- Sun X, Cahill J, Van Hautegeem T, Feys K, Whipple C, Novák O, Delbare S, Versteede C, Demuyneck K, De Block J, et al** (2017) Altered expression of maize PLASTOCHRON1 enhances biomass and seed yield by extending cell division duration. *Nat Commun* **8**: 1–11
- Sussex, I. M. and Steeves TA** (1989) *Patterns in Plant Development*, 2nd ed. doi: <https://doi.org/10.1017/CBO9780511626227>
- Vernoud V, Laigle G, Rozier F, Meeley RB, Perez P, Rogowsky PM** (2009) The HD-ZIP IV transcription factor OCL4 is necessary for trichome patterning and anther development in maize. *Plant J* **59**: 883–894
- Vickovic S, Eraslan G, Salmén F, Klughammer J, Stenbeck L, Schapiro D, Äijö T, Bonneau R, Bergensträhle L, Navarro JF, et al** (2019) High-definition spatial transcriptomics for in situ tissue profiling. *Nat Methods* **16**: 987–990
- Whipple CJ, Kebrom TH, Weber AL, Yang F, Hall D, Meeley R, Schmidt R, Doebley J, Brutnell TP, Jackson DP** (2011) grassy tillers1 promotes apical dominance in maize and responds to shade signals in the grasses. *Proc Natl Acad Sci U S A* **108**: E506–12
- Wilbrey-Clark A, Roberts K, Teichmann SA** (2020) Cell Atlas technologies and insights into tissue architecture. *Biochem J* **477**: 1427–1442
- Yang F, Bui HT, Pautler M, Llaca V, Johnston R, Lee B, Kolbe A, Sakai H, Jackson D** (2015) A maize glutaredoxin gene, abphyl2, regulates shoot meristem size and phyllotaxy. *Plant Cell* **27**: 121–131
- Zhang X, Madi S, Borsuk L, Nettleton D, Elshire RJ, Buckner B, Janick-Buckner D, Beck J, Timmermans M, Schnable PS, et al** (2007) Laser Microdissection of Narrow Sheath Mutant Maize Uncovers Novel Gene Expression in the Shoot Apical Meristem. *PLOS Genet* **3**: e101

Zhou X, Li S, Zhao Q, Liu X, Zhang S, Sun C, Fan Y, Zhang C, Chen R (2013) Genome-wide identification, classification and expression profiling of nicotianamine synthase (NAS) gene family in maize. *BMC Genomics* **14**: 238

Zhu M, Chen W, Mirabet V, Hong L, Bovio S, Strauss S, Schwarz EM, Tsugawa S, Wang Z, Smith RS, et al (2020) Robust organ size requires robust timing of initiation orchestrated by focused auxin and cytokinin signalling. *Nat Plants* **6**: 686–698

Zöllner NR, Bezruczyk M, Laureyns R, Nelissen H, Simon R, Frommer WB (2021) An RNA in situ hybridization protocol optimized for monocot tissue. *STAR Protoc* **2**: 100398

## Figure legends

**Figure 1: Individual and combined expression patterns visualized by ISS in longitudinal sections through the maize SAM.** A) Annotation of the tissue on a longitudinal section through the maize shoot apex, stained by DAPI, on which the expression domains of B-F are assayed. Expression patterns of B) *RS1*; C) *OCL4*; D) *PIN1a*; E) *DRP4a*. F) Composite image of *RS1*, *OCL4* and *DRP4a* expression patterns. G) Zoomed inset of *RS1*, *OCL4* and *DRP4a* in the maize SAM.

**Figure 2: Validation of the ISS data with single gene mRNA *in situ* hybridizations.** (A-B) *PIN1a* is expressed in vascular tissue; C-D) *AN3/GIF1* is expressed in the meristem and developing leaves; E-F) *GRF1* is expressed in young leaves and in vascular tissue; G-H) *CUC2* is expressed at the leaf-meristem boundaries; I-J) *BE1* is expressed in leaf primordia and at the base of young developing leaves; K-L) *LAX2* is expressed in developing vascular bundles; M-N) *DRP4a* is expressed at the tip of the meristem and O-P) *H4* expression marks actively dividing cells. Background signal in ISS pictures are DAPI stained nuclei.

**Figure 3: Combined expression patterns obtained by ISS in longitudinal section through the maize shoot apex.** A) Composite image of *LOG7* (orange), *DRP4a* (yellow), *AGO18a* (purple), *YAB14* (blue) and *YAB9* (green). B) Composite image of boundary genes *CUC2* (yellow), *CUC3* (green), *D11-LIKE* (red), *BA1* (blue), *BAF1* (purple). C) Zoomed inset of B. D) Image of vascular markers, *PIN1a* (blue), *BIF1* (yellow), *GRX8C* (red), *LAX2* (orange), *NAS3* (purple), *ZCN1/3* (dark blue). E) Zoomed inset of D. Background signal are DAPI stained nuclei.

**Figure 4: Expression patterns of *PLA1* obtained through ISH and ISS in the maize shoot apex.** A) Expression pattern of *PLA1* obtained by RNA *in situ* hybridization in a longitudinal section of a B104 SAM. B) Expression pattern of *PLA1* obtained by ISS in a longitudinal section of a B104 SAM. C) Expression pattern of *PLA1* obtained through RNA *in situ* hybridization on a transverse section of a B104 SAM. D) *PLA1* expression pattern in transverse sections of a B104 SAM using ISS. E) Heat-map of cells expressing *PLA1* in a B104 shoot apex. F) *PLA1* is more broadly expressed in the stem, vascular bundles and in the leaves (black arrowheads) in the *GA2ox::PLA1* overexpression line as compared with the expression in B104. Background signal in ISS pictures are either DAPI or Calcofluor White (CW) stained cells.

**Figure 5: ISS on segmented cells expressing indeterminate and determinate cell types.** A) Cells expressing *RS1* are depicted in purple. B) Determinate leaf epidermal cells expressing *OCL4* are depicted in cyan. C) Combination of cells expressing *RS1* (purple) and *OCL4* (cyan) illustrate the sharp

demarcation of indeterminate to determinate tissues. D-E) Expression of *PLA1* (yellow) is located at the boundary between indeterminate (purple) and determinate tissues (cyan). Brown cells depict express both *PLA1* and *RS1*, cells expressing both *PLA1* and *OCL4* are depicted in green, cells expressing both *RS1*, *PLA1* and *OCL4* are depicted in dark green. Background signal is Calcofluor White (CW) stained cells

**Figure 6: Comparison of multi-gene expression patterns obtained by ISS.** Expression patterns obtained in the shoot apex from: A) *PLA1* (yellow), *CUC2* (blue) and *D11-LIKE* (red). B) *PLA1* (yellow), *CUC2* (blue), *D11-LIKE* (red), *BA1* (magenta) and *BAF1* (orange). C) *AN3/GIF1* (green), *PLA1* (yellow), *D11-LIKE* (red), *CUC2* (blue). D) Zoomed-in region of C. E) *PLA1* (yellow) and *PIN1a* (blue). Background signal are DAPI stained nuclei.

**Supplemental Figure S1: Background fluorescence check on FFPE maize shoot apex sections.** A-C) visualization of nuclei using DAPI-stain. A) Bright field image depicting maize shoot apex, B) DAPI signal highlighting nuclei and C) merged images. D-F) *DR5::RFP* signal, D) brightfield image of the maize SAM, E) *DR5::RFP* signal, F) merged images.

**Supplemental Figure S2: Quality control amplified spots in a longitudinal section of the maize SAM.** A) DAPI-stain depicting individual nuclei, B) Visualization of ISS spots using the anchor probe, C) merged image of DAPI and ISS spots and D) ISS spots of 90-genes are decoded and genes are assigned a specific color and symbol.

**Supplemental Figure S3: Specific expression patterns visualized by ISS in a longitudinal section of the maize SAM.** A) *KN1* expression is observed in the meristem and stem. B) *GA2OXIDASE1* (*GA2ox1*) is expressed at the base of developing leaves. C) *AGO18a* is expressed in the central zone of the meristem. D) *KNOX3* is specifically expressed at the boundary between stem and leaf. E) *BARELY ANY MERISTEM1d* (*BAM1d*) is expressed at the stem-leaf boundary and in young developing leaves. F) *JACALIN RELATED LECTIN* (*JRL*) is specifically expressed in mesophyll cells in the leaf and in the stem. G) *CUC2* is specifically expressed at the boundaries between stem and leaf. H) *TREHALOSE-6-PHOSPHATE PHOSPHATASE4* (*TTP4*) is specifically expressed at the base of the leaf.

**Supplemental Figure S4: Illustration of the SAM before and after segmentation.** A) Composite image of DAPI stain depicting nuclei and cell-wall stain depicting plant cell walls. B) Overlay obtained segmented cells on composite SAM image.

**Supplemental Figure S5: Evaluating the reproducibility of the ISS technology.** The count number for every gene was normalized relative to the total number of counts and the  $R^2$  between the different sections was calculated.

**Supplemental Figure S6: Evaluating the expression pattern of *PLA1* over different replicates.** A-B) *PLA1* expression pattern in the first repeat (Pilot). C-D) *PLA1* expression pattern in the first repeat (slide-A). E-F) *PLA1* expression pattern in the first repeat (slide-B). Background signal are DAPI stained nuclei.

**Supplemental Figure S7: Validation of the ISS data with single gene mRNA *in situ* hybridizations.** (A-B) *GE1* is expressed in developing leaf primordia; C-D) *GIF2* is expressed in the vasculature; E-F) *GIF3* is expressed in young leaves and in vascular tissue; G-H) *GIF4* is expressed in the developing leaf primordia; I-J) *GRF10* is expressed in vascular tissue; K-L) *KLU-1* is expressed in developing vascular bundles; M-N) *KLU-2* is expressed is expressed in developing vascular bundles and the base of developing leaf primordia; O-P) *KN1* expression marks meristematic cells and Q-R) *VP8* is expressed in vascular tissue. Background signal in ISS pictures are DAPI stained nuclei.

**Supplemental Figure S8: Histogram depicting the distribution of gene counts per cell over 12267 cells.**

**Supplemental Figure S9: Expression pattern of *HISTONE H4* as obtained using ISS.** A) Expression in the shoot apex. B) Expression in a close-up of region marked by the white box in A. C) Expression in a close-up of region marked by the white box in A, with addition of a cell wall marker.

**Supplemental Figure S10: Comparison expression patterns of *CUC2* in the maize shoot apex.** A) Expression patterns of *CUC2* as obtained by amplification of probes targeting *CUC2*. B) Expression pattern of *CUC2* as observed by ISS.

**Supplemental Figure S11: Specific expression patterns obtained using ISS in the shoot apex.** Expression patterns of genes expressed in the boundary regions: *CUC2* (yellow) and *CUC3* (green), *D11-LIKE* (red), *BA1* (light blue), *BAF1* (purple), *TB1* (orange) and *GT1* (dark blue). B) Transverse section depicting expression of cell-specific marker genes: *OCL4* (yellow), *MWP4* (orange), *ARF3* (purple), *RLD1* (green) and *JRL* (blue). C-D) Zoomed regions of B. C) Zoom in of developing leaf primordia. D) Zoom in on the region of the maize SAM.

**Supplemental Figure S12: Phenotype of *pla1* mutant.** A) Image representing a WT and *pla1-2* mutant of the same age. B) The final leaf length of leaf 4 is decreased in *pla1-1* mutants. C) Quantitative measurement of number of leaves observed during a 11 day growth-period in *pla1-2* mutants. D) *pla1-2* mutants have a slightly reduced LER and a strong reduced LED. Black asterisk : significant difference  $P < 0.05$ , Student's T-test. White asterisk: an additional leaf in the *pla1* mutant.  $N \geq 13$ . Error bars represent standard error.

**Supplemental Figure S13: Expression patterns of *PLA1*, *KN1* and *YAB15* visualized through ISH.** A) Expression pattern of *PLA1* is localized at the junction between the center of the ear and developing spikelets. B) *PLA1* accumulates at the boundary between differentiated lateral organs and meristematic cells in spikelets as depicted by *KN1* expression (C) and *YAB15* (D). Gl: Glume; Pa: Palea; Ufm: Upper floral meristem; Lfm: Lower floral meristem; Le: Lemma.

## Figures

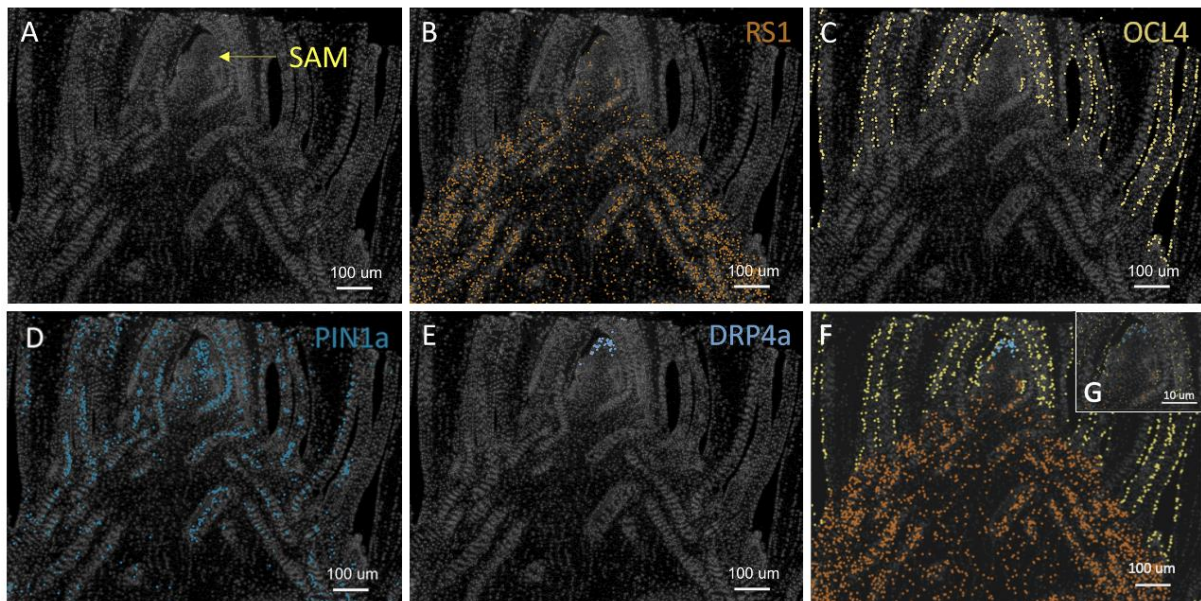


**Figure 1: Individual and combined expression patterns visualized by ISS in longitudinal sections through the maize SAM.** A) Annotation of the tissue on a longitudinal section through the maize shoot apex, stained by DAPI, on which the expression domains of B-F are assayed. Expression patterns of B) *RS1*; C) *OCL4*; D) *PIN1a*; E) *DRP4a*. F) Composite image of *RS1*, *OCL4* and *DRP4a* expression patterns. G) Zoomed inset of *RS1*, *OCL4* and *DRP4a* in the maize SAM.

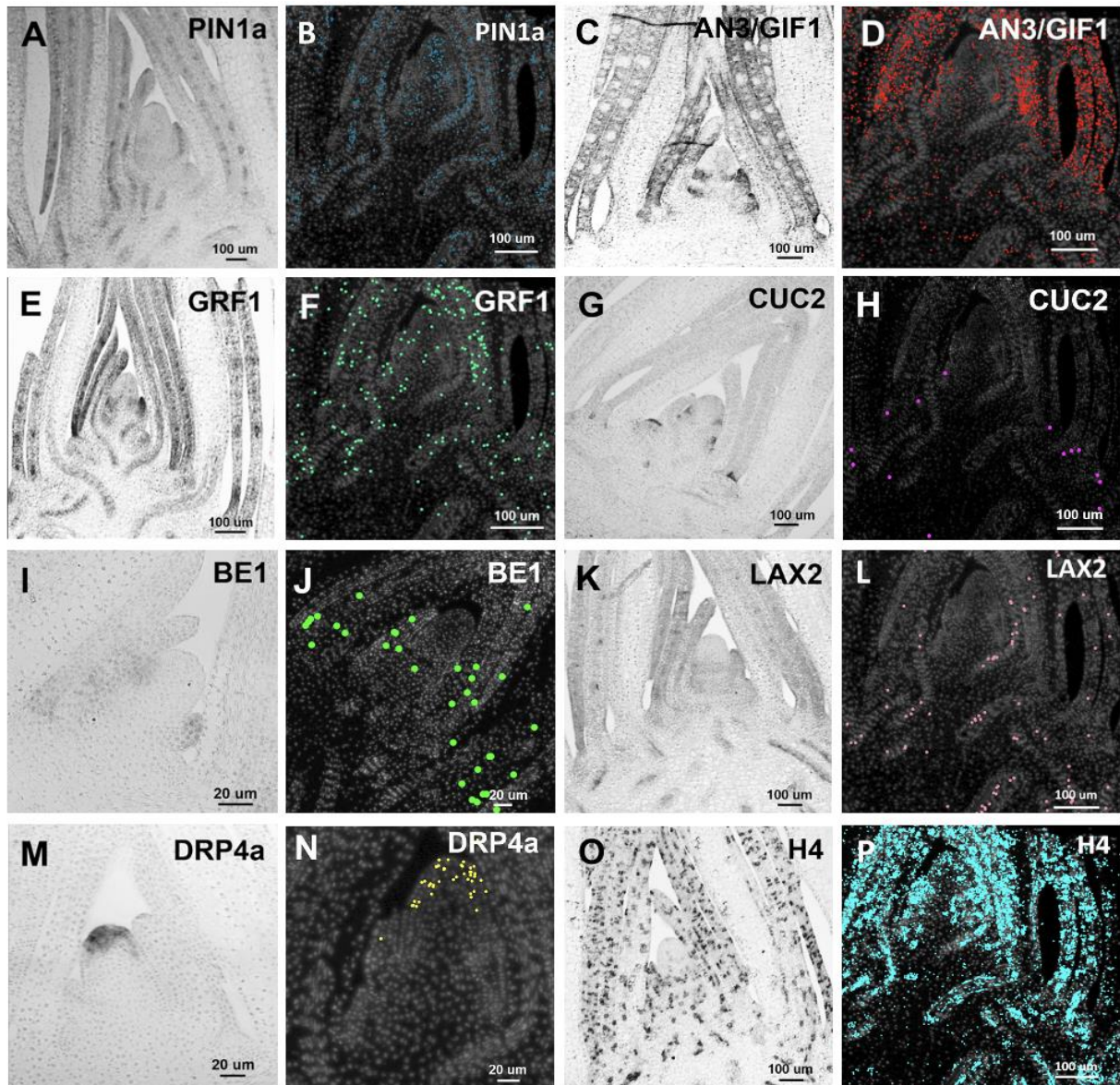


**Figure 2: Validation of the ISS data with single gene mRNA *in situ* hybridizations.** (A-B) *PIN1a* is expressed in vascular tissue; C-D) *AN3/GIF1* is expressed in the meristem and developing leaves; E-F) *GRF1* is expressed in young leaves and in vascular tissue; G-H) *CUC2* is expressed at the leaf-meristem boundaries; I-J) *BE1* is expressed in leaf primordia and at the base of young developing leaves; K-L) *LAX2* is expressed in developing vascular bundles; M-N) *DRP4a* is expressed at the tip of the meristem and O-P) *H4* expression marks actively dividing cells. Background signal in ISS pictures are DAPI stained nuclei.

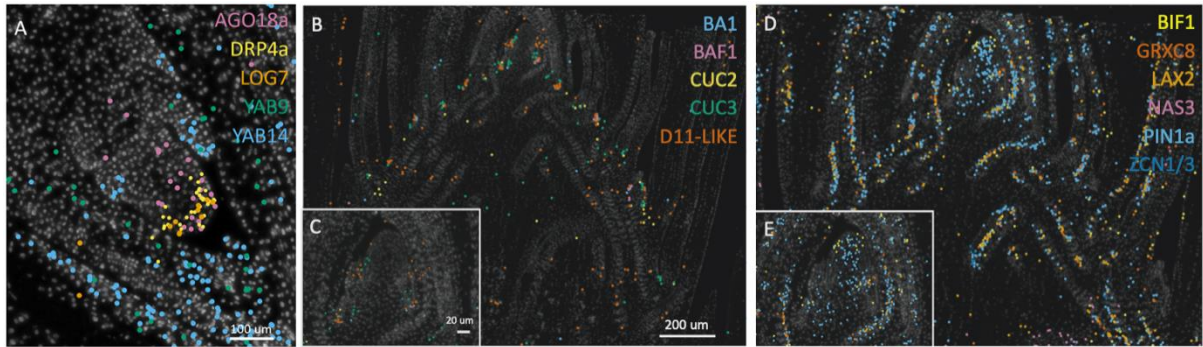


**Figure 3: Combined expression patterns obtained by ISS in longitudinal section through the maize shoot apex.** A) Composite image of *LOG7* (orange), *DRP4a* (yellow), *AGO18a* (purple), *YAB14* (blue) and *YAB9* (green). B) Composite image of boundary genes *CUC2* (yellow), *CUC3* (green), *D11-LIKE* (red), *BA1* (blue), *BAF1* (purple). C) Zoomed inset of B. D) Image of vascular markers, *PIN1a* (blue), *BIF1* (yellow), *GRX8C* (red), *LAX2* (orange), *NAS3* (purple), *ZCN1/3* (dark blue). E) Zoomed inset of D. Background signal are DAPI stained nuclei.

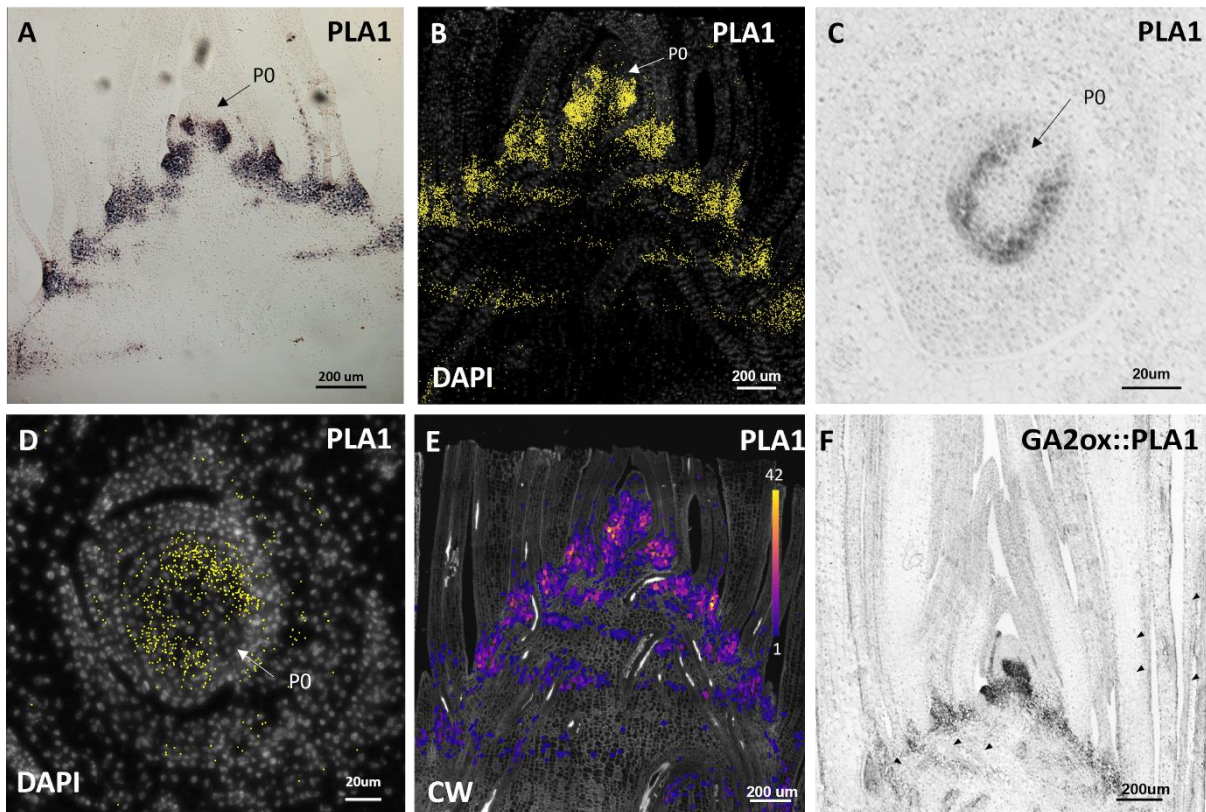


**Figure 4: Expression patterns of *PLA1* obtained through ISH and ISS in the maize shoot apex.** A) Expression pattern of *PLA1* obtained by RNA *in situ* hybridization in a longitudinal section of a B104 SAM. B) Expression pattern of *PLA1* obtained by ISS in a longitudinal section of a B104 SAM. C) Expression pattern of *PLA1* obtained through RNA *in situ* hybridization on a transverse section of a B104 SAM. D) *PLA1* expression pattern in transverse sections of a B104 SAM using ISS. E) Heat-map of cells expressing *PLA1* in a B104 shoot apex. F) *PLA1* is more broadly expressed in the stem, vascular bundles and in the leaves (black arrowheads) in the *GA2ox::PLA1* overexpression line as compared with the expression in B104. Background signal in ISS pictures are either DAPI or Calcofluor White (CW) stained cells.

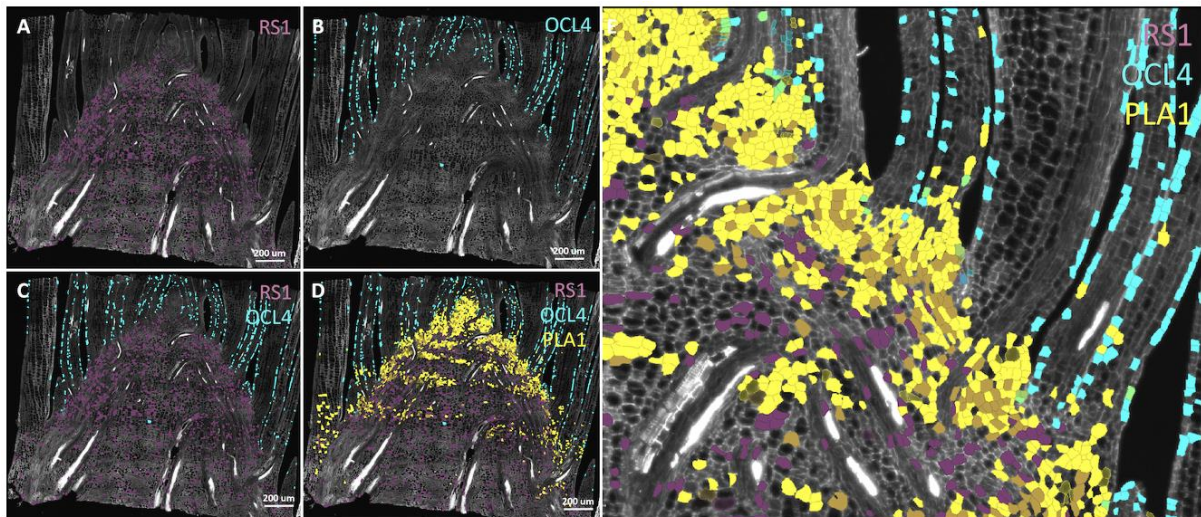


**Figure 5: ISS on segmented cells expressing indeterminate and determinate cell types.** A) Cells expressing *RS1* are depicted in purple. B) Determinate leaf epidermal cells expressing *OCL4* are depicted in cyan. C) Combination of cells expressing *RS1* (purple) and *OCL4* (cyan) illustrate the sharp demarcation of indeterminate to determinate tissues. D-E) Expression of *PLA1* (yellow) is located at the boundary between indeterminate (purple) and determinate tissues (cyan). Brown cells depict express both *PLA1* and *RS1*, cells expressing both *PLA1* and *OCL4* are depicted in green, cells expressing both *RS1*, *PLA1* and *OCL4* are depicted in dark green. Background signal is Calcofluor White (CW) stained cells

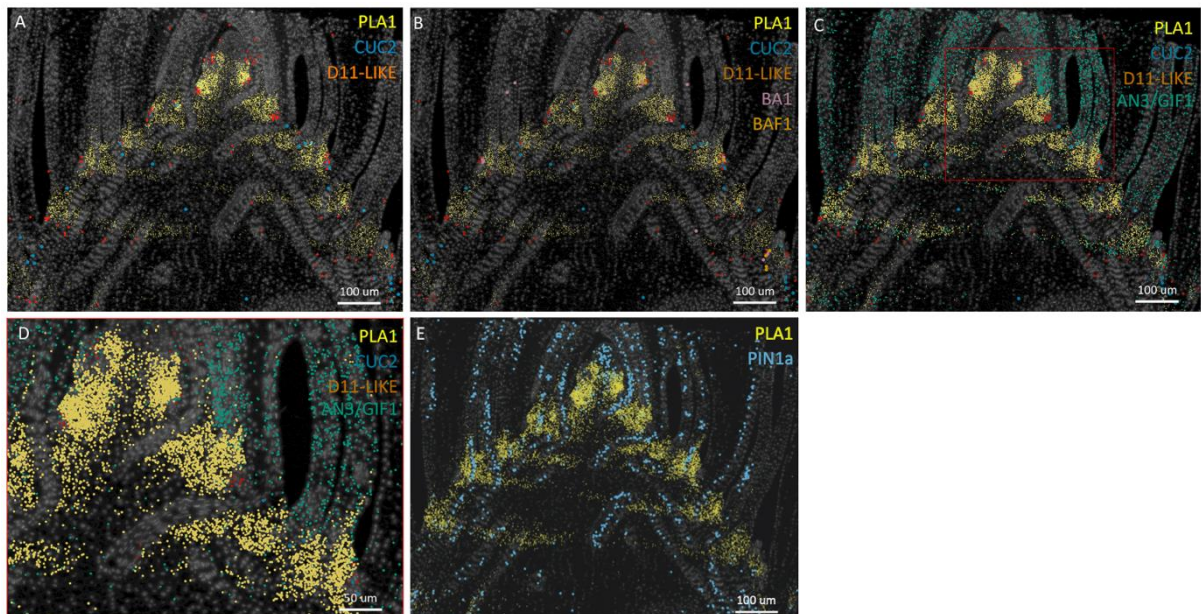


**Figure 6: Comparison of multi-gene expression patterns obtained by ISS.** Expression patterns obtained in the shoot apex from: A) *PLA1* (yellow), *CUC2* (blue) and *D11-LIKE* (red). B) *PLA1* (yellow), *CUC2* (blue), *D11-LIKE* (red), *BA1* (magenta) and *BAF1* (orange). C) *AN3/GIF1* (green), *PLA1* (yellow), *D11-LIKE* (red), *CUC2* (blue). D) Zoomed-in region of C. E) *PLA1* (yellow) and *PIN1a* (blue). Background signal are DAPI stained nuclei.